CHEMISTRY OF MATERIALS

Article

pubs.acs.org/cm

Synthesis and Characterization of CIT-13, a Germanosilicate Molecular Sieve with Extra-Large Pore Openings

Jong Hun Kang,[†] Dan Xie,[‡] Stacey I. Zones,[‡] Stef Smeets,[§] Lynne B. McCusker,[§,⊥] and Mark E. Davis*[,†]

[†]Division of Chemistry and Chemical Engineering, California Institute of Technology, Pasadena, California 91125, United States

[‡]Chevron Energy Technology Company, 100 Chevron Way, Richmond, California 94802, United States

[§]Department of Materials and Environmental Chemistry, University of Stockholm, Svante Arrhenius väg 16C, SE-106 91 Stockholm, Sweden

[⊥]Department of Materials, ETH Zurich, CH-8093 Zurich, Switzerland

Supporting Information

ABSTRACT: The synthesis of the germanosilicate CIT-13, a molecular sieve that is the first to have a two-dimensional (2D) pore system possessing pores that are bounded by 14- and 10-rings, is accomplished using a family of monoquaternary, benzyl-imidazolium organic structure-directing agents (OSDAs) in aqueous media containing fluoride. CIT-13 is prepared using either hydrogen fluoride (HF) or ammonium fluoride (NH_4F). The structure refinement suggests that most of the Ge atoms are located in the *d4r* (double-4-rings) units, and that there are framework disorders in the arrangement of those *d4r* units. Other characterizations of CIT-13 such as ^{29}Si MAS NMR spectra, Ar-adsorption isotherms, and so forth are presented and compared to those of IM-12 (**UTL**), a previously reported germanosilicate with 14- and 12-ring pores.

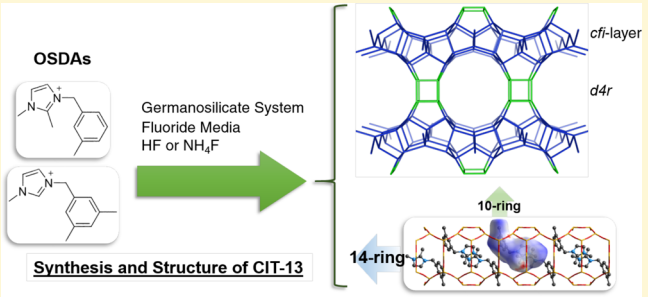

1. INTRODUCTION

Zeolites, a class of open framework aluminosilicates, and their analogs are popular heterogeneous catalysts in the petrochemical industry because of their high thermal stability and shape-selective properties. The latter arise from the well-defined pore systems in these crystalline materials, whose channel- and pore-wall compositions are tunable.[1−3] The extra-large-pore zeolite frameworks with channels defined by more than 12 Si or other tetrahedrally coordinated framework atoms (T atoms) are of particular interest, because they can accommodate and process larger feedstock molecules.[4−6]

Many such extra-large-pore frameworks are found in the germanosilicate (Si/Ge ratio >3) family.[3,4] Germanium is known to play a stabilizing role in the formation of small composite building units (CBUs) with high geometric constraints such as the double 4-ring (*d4r*) or double 3-ring (*d3r*).[6−8] This concept led to a synthesis route for producing a large array of new molecular sieves with low framework densities and extra-large pores.[9−16] Typically, fluoride is used as the mineralizing agent, that further stabilizes the formation of *d4r* units.[16−18] However, the inclusion of Ge also introduces a structural weakness that reduces the thermal and hydrothermal stability of the molecular sieve, so it is desirable to minimize its content. To this end, some researchers have developed experimental methods to replace Ge with Al,[19] Si,[20] or Ti[21] in a postsynthesis treatment, while others have exploited the preferential occupation of Ge in the *d4r* units to invoke an inverse sigma transformation to create high-silica molecular sieves with new frameworks that are not accessible by conventional synthesis methods.[22−24] The germanosilicate IM-12 with the **UTL** framework type (3-letter codes are assigned to designate framework types by the Structure Commission of the International Zeolite Association)[25] has been a prime starting material for exploring such transformations via the ADOR (Assembly-Dissembly-Organization-Reassembly) process, yielding the IPC-2 (**OKO**)/IPC-4 (**PCR**)[23] and IPC-9/IPC-10[26] pairs.

As part of a screening program to synthesize germanosilicate molecular sieves using mono and diquaternary ammonium structure-directing agents derived from benzyl imidazolium, the new molecular sieve, CIT-13, was produced.[27] The framework structure found in that study can be described in terms of dense layers, similar to those found in the CIT-5 (**CFI**) framework structure (hereafter called cfi-layers),[28] connected via *d4r* units to form a 2-dimensional channel system delimited by 14- and 10-ring pore openings (the term n-ring stands for the number of tetrahedral atoms defining the size of a channel)[25] between the layers (Figure 1). The cfi-layers contain cas, mtt, and ton CBUs. For comparison, adjacent layers in the **CFI** framework, are shifted by half a unit cell along the 14-ring channel and are

Received: June 17, 2016
Revised: August 17, 2016
Published: August 18, 2016

DOI: 10.1021/acs.chemmater.6b02468
Chem. Mater. 2016, 28, 6250−6259

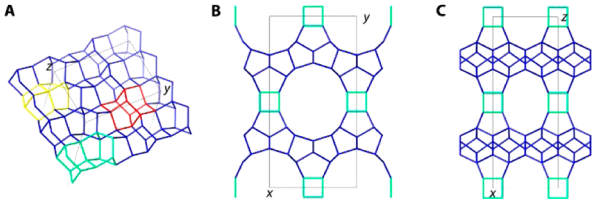

Figure 1. Idealized framework structure of CIT-13. (A) *cfi*-layer in the *y*−*z* plane with the *cas* (red), *mtt* (yellow), and *ton* (green) composite building units highlighted, (B) view along the [001] direction showing the 14-ring pore, and (C) view along the [010] direction showing the 10-ring pore. In (B) and (C), the *d4r* units connecting the *cfi*-layers (blue) have been highlighted in green. Bridging O atoms have been omitted for clarity.

connected by double zigzag chains to form 1-dimensional 14-ring channels. The CIT-13 framework structure bears a striking resemblance to that of IM-12, where dense layers similar (but not identical) to those in the **FER** framework are connected via *d4r* units to create a 14- and 12-ring pore system between the layers. We anticipate, therefore, that CIT-13 will exhibit a chemistry similar to that of the very versatile IM-12, and are currently exploring this possibility.

Here, we report synthetic methods for preparing CIT-13, its structural refinement and the characterization of its properties. The crystallization of silica-based molecular sieves is typically a very complex process that depends on a large number of variables, such as alkalinity, structure of the organic structure-directing agent (OSDA), water content, temperature, and mineralizer used.[28,29] Therefore, we performed a systematic investigation of the synthetic conditions that form CIT-13, and developed a synthesis protocol using ammonium fluoride (NH_4F) to avoid the use of concentrated hydrogen fluoride (HF). To better understand the synthesis and potential applications of CIT-13, the samples were characterized by thermogravimetric analysis (TGA), ^{29}Si magic-angle spinning (MAS) nuclear magnetic resonance (NMR) and cryogenic argon-adsorption, and the results compared with the corresponding data from IM-12 (**UTL**). To confirm the framework structure of CIT-13, and to investigate the distribution of Ge in the framework and the location of the OSDA in the pores, we also undertook a full structure analysis using synchrotron X-ray powder diffraction (XPD) data.

2. EXPERIMENTAL SECTION

2.1. Synthesis of Organic Structure-Directing Agents (OSDA). *2.1.1. Preparation of OSDA 1: 1,2-Dimethyl-3-(3-methylbenzyl)imidazolium Hydroxide.* First, 14.4 g (150 mmol) of 1,2-dimethylimidazole (98%, Sigma-Aldrich) was dissolved in 300 mL of toluene and heated up to 45 °C. While vigorously stirring, 21.1 g (150 mmol) of 3-methylbenzyl chloride (98%, Sigma-Aldrich) was added dropwise. After 30 min of additional stirring, the temperature was increased to 105 °C and the reaction was allowed to proceed for 24 h. After that, the reaction mixture was cooled and filtered. The chloride salt obtained was washed repeatedly with 4 L of diethyl ether and dried under vacuum for 12 h. The chloride anions were exchanged with hydroxyl anions using OH-form styrene-divinylbenzene (DVB)-matrix ion-exchange resin (DOWEX MARATHON). ^{1}H NMR (500 MHz, $CDCl_3$): δ 7.79 (d, 1H), 7.58 (d, 1H), 7.29 (m, 1H), 7.19 (m, 1H), 7.11 (m, 1H), 7.10 (m, 1H), 5.49 (s, 2H), 4.03 (s, 3H), 2.81 (s, 3H), 2.37 (s, 3H). ^{13}C NMR (125 MHz, $CDCl_3$): δ 144.29, 139.37, 132.79, 129.92, 129.29, 128.60, 125.10, 122.96, 121.73, 52.46, 35.90, 21.36, 10.90.

2.1.2. Preparation of OSDA 2: 1-Methyl-3-(3-methylbenzyl)-imidazolium Hydroxide. First, 14.4 g (150 mmol) of 1-methylimidazole (98%, Sigma-Aldrich) was dissolved in 300 mL of toluene and heated up to 45 °C. While vigorously stirring, 21.1 g (150 mmol) of 3-methylbenzyl chloride (98%, Sigma-Aldrich) was added dropwise. After 30 min of additional stirring, the temperature was increased to 105 °C and the reaction was allowed to proceed for 24 h. After that, the reaction mixture was cooled in a dry ice bath since this imidazolium salt exists as a liquid salt at room temperature. A cold filtration was performed to isolate the product in solid form. The chloride salt obtained was washed repeatedly with 4 L of cold diethyl ether and dried under vacuum for 12 h. The ion-exchange was conducted as described above. ^{1}H NMR (500 MHz, $CDCl_3$): δ 10.54 (s, 1H), 7.64 (t, 1H), 7.32 (m, 1H), 7.14 (m, 3H), 7.05 (m, 1H), 5.42 (s, 2H), 3.97 (s, 3H), 2.22 (s, 3H). ^{13}C NMR (125 MHz, $CDCl_3$): δ 139.14, 137.42, 133.02, 130.04, 129.28, 129.12, 125.77, 123.92, 121.78, 53.07, 36.46, 21.21.

2.1.3. Preparation of OSDA 3: 1,2-Dimethyl-3-(3,5-dimethylbenzyl)imidazolium Hydroxide. First, 12.3 g (150 mmol) of 1,2-dimethylimidazole (98%, Sigma-Aldrich) was dissolved in 300 mL of toluene in an ice bath. While vigorously stirring, 29.9 g (150 mmol) of 3,5-dimethylbenzyl bromide (98%, Alfa Aesar) was added. After 30 min of additional stirring, the temperature was slowly increased to 105 °C and the reaction was allowed to proceed for 15 h. After that, the reaction mixture was cooled and filtered. The chloride salt obtained was washed repeatedly with 4 L of diethyl ether and dried under vacuum for 12 h. The ion-exchange was conducted as described above. ^{1}H NMR (500 MHz, $CDCl_3$): δ 7.77 (d, 1H), 7.49 (d, 1H), 6.99 (m, 1H), 6.89 (m, 2H), 5.41 (s, 2H), 4.03 (s, 3H), 3.19 (s, 3H), 2.31 (s, 6H). ^{13}C NMR (125 MHz, $CDCl_3$): δ 144.29, 139.19, 132.55, 130.81, 125.71, 122.92, 121.61, 52.57, 36.19, 21.23, 11.38.

2.1.4. Preparation of OSDA 4: 1-Methyl-3-(3,5-dimethylbenzyl)-imidazolium Hydroxide. First, 12.3 g (150 mmol) of 1,2-dimethylimidazole (98%, Sigma-Aldrich) was dissolved in 300 mL of toluene in an ice bath. While vigorously stirring, 29.9 g (150 mmol) of 3,5-dimethylbenzyl bromide (98%, Alfa Aesar) was added. After 30 min of additional stirring, the temperature was slowly increased to 105 °C and the reaction was allowed to proceed for 15 h. After that, the reaction mixture was cooled and filtered. The bromide salt obtained was washed repeatedly with 4 L of diethyl ether and dried under vacuum for 12 h. The ion-exchange was conducted as described above. ^{1}H NMR (500 MHz, $CDCl_3$): δ 10.46 (td, 1H), 7.53 (t, 1H), 7.27 (d, 1H), 7.00 (dm, 3H), 5.44 (s, 2H), 4.09 (s, 3H), 2.28 (s, 6H). ^{13}C NMR (125 MHz, $CDCl_3$): δ 139.23, 137.34, 132.55, 131.17, 126.59, 123.65, 121.71, 53.44, 36.78, 21.18.

2.2. Synthesis of Germanosilicate CIT-13 in Fluoride Media. The synthesis of CIT-13 was performed in the same way as reported previously.[27] Specifically, the gel compositions used were $x/(x+1)$ SiO_2:$1/(x+1)$ GeO_2:y(OSDA)$^+$$OH^-$: yHF:5−15 H_2O where x is the Si/Ge molar ratio of the gel. The values of y were tested within 0.5−0.75. (The condition with x = 4, y = 0.5, and T = 160 °C is referred to as the reference condition in this work.) The desired amount of germanium(IV) oxide (GeO_2, Strem, 99.999%) was dissolved in the desired amount of OSDA aqueous solution and tetraethyl orthosilicate (TEOS, Alfa Aesar, 98%) in a 23 mL PTFE liner (Parr Instrument). The mixture was stirred for 12 h in order to hydrolyze all TEOS and dried under a continuous air flow to evaporate excess water and ethanol until the gel became very viscous. The equivalent amount of concentrated hydrofluoric acid (HF, Sigma-Aldrich, 48 wt %) was added dropwise and thoroughly mixed using a PTFE spatula. After this HF-mixing, the mixture became powdery. After an additional 2 days of drying, the desired amount of distilled water and seed material (2−3 wt % of total mixture, optional) was added and the mixture was mixed thoroughly. The seed material was as-synthesized CIT-13 from the reference condition. The PTFE liner containing the mixture was firmly clad with a Parr still reactor and put in a convection oven. The crystallization temperature was typically 160 °C, but other temperatures in a range from 140 to 175 °C have also been used. The crystallization was performed under static conditions and monitored for at least 1 month. The resultant CIT-13 powder was washed carefully with distilled water, methanol, and acetone, and dried in a 70 °C convection oven before being characterized.

DOI: 10.1021/acs.chemmater.6b02468
Chem. Mater. 2016, 28, 6250−6259

2.3. Synthesis of Germanosilicate CIT-13 Using Ammonium Fluoride (NH_4F). The gel composition for the NH_4F-protocol was the same as for the HF-protocol described above, except that the molar-equivalent amount of NH_4F was used in place of HF. The desired amounts of GeO_2 and NH_4F were dissolved in the OSDA aqueous solution and TEOS in a 23 mL PTFE liner. The mixture was stirred for 12 h in order to hydrolyze all TEOS, and dried under a continuous air flow to evaporate excess water, ammonia, and ethanol until the gel became completely powdery. Then, water was added to the desired level. The PTFE liner containing the mixture was firmly clad with a Parr still reactor and put in a convection oven at 160 °C. The rest of the protocol is the same as above.

2.4. Synthesis of Germanosilicate IM-12 in Hydroxide Media. The germanosilicate IM-12 (**UTL**) was also synthesized for comparison with CIT-13. A spiro-quaternary ammonium, (6*R*,10*S*)-6,10-dimethyl-5-azaspiro[4.5]decanium hydroxide, was used as the OSDA for the synthesis of IM-12. This OSDA was prepared according to the protocol described in literature.[16,30] The IM-12 germanosilicate was synthesized solvothermally using hydroxide (OH^-) medium. The gel composition was 0.667 SiO_2:0.333 GeO_2:0.25 $(OSDA)^+OH^-$:30 H_2O. The gel mixture was prepared by dispersing the desired amounts of silica (Cab-o-Sil) and GeO_2 in $(OSDA^+)OH^-$ solution and the water content was adjusted by simply adding the equivalent amount of distilled water. The crystallization was performed at 175 °C for 14 day in a 23 mL Parr reactor. The rinsing step of the crystalline IM-12 material was the same as that described above for CIT-13.

2.5. Characterization. Lab XPD data were collected on all samples using a Rigaku Miniflex II diffractometer with Cu Kα radiation (wavelength = 1.5418 Å). Synchrotron XPD data were collected on an as-synthesized sample of CIT-13 from the reference condition in 0.3 mm capillaries on the MS-Powder beamline at the Swiss Light Source in Villigen, Switzerland[31] using a wavelength of 0.7764 Å and a Mythen II detector. Three-dimensional electron diffraction data were also collected on 3 crystals of CIT-13 using the rotation electron diffraction (RED) technique.[32] The RED software was installed on a JEOL 2010 microscope operating at 200 kV, and data were collected over a tilt range of ±50° with a tilt step of 0.50° for the three sets, the exposure time is 2 s per tilt step.

Scanning electron microscopy (SEM) was conducted on a FE-SEM microscope (ZEISS 1550VP), and the elemental analysis of the crystals was performed using an Oxford X-Max SDD X-ray Energy Dispersive Spectrometer (EDS) system. The ^1H and ^{13}C solution-phase NMR spectra of the four OSDAs were obtained using a Varian 500 MHz Spectrometer with auto-x pfg broadband probe with the carrier frequencies 500 and 125 MHz, respectively. The organic salts were dissolved in $CDCl_3$ in their halide forms for the solution-phase NMR. The ^{13}C and ^{29}Si MAS solid-state NMR spectra were obtained using a Bruker Avance 500 MHz spectrometer. The powdered samples of CIT-13 were charged in a 4 mm Bruker zirconia (ZrO_2) rotor, and the MAS rate was 8−12 kHz. The cryogenic argon adsorption isotherms were obtained using a Quantachrome Autosorb iQ at 87.45 K.

3. RESULTS

3.1. Synthesis Conditions. We recently reported the first synthesis of CIT-13 using a benzylimidazolium-derived OSDA (OSDA 1) and fluoride medium.[27] With the same OSDA, the crystallization conditions for CIT-13 were systematically tested, and the crystallization kinetics were obtained for various Si/Ge ratios of the gel, water content, presence or absence of seeding material, amounts of $OSDA^+OH^-$/HF, and crystallization temperatures. A family of OSDAs with closely related structures (Figure 2) was also explored with varying levels of Ge. In total, 33 sets of conditions were tested and these are summarized in Table 1. The purity of the samples obtained was determined qualitatively from the XPD profiles.

Crystallization conditions that produce high quality CIT-13 product reproducibly were determined to be 0.8 SiO_2:0.2 GeO_2:0.5 $(OSDA\ 1)^+OH^-$:0.5 HF:10 H_2O at 160 °C. With this set of crystallization parameters (hereafter the reference conditions), an impurity-free CIT-13 sample can be obtained after 14−21 days of crystallization time. The morphology of the CIT-13 crystals resembles that of **UTL**-framework materials (Figure S1−S3).[16]

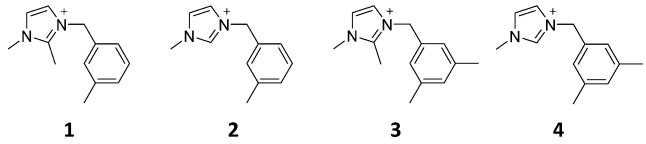

Figure 2. Organic structure-directing agents (OSDAs) used in this study to produce CIT-13 in a germanosilicate system and fluoride medium.

Other crystallization conditions also yielded excellent CIT-13 products and several of the XPD profiles from these syntheses are displayed in Figure 3. The CIT-13 samples synthesized under these conditions showed good thermal stability (Figure S4).The Si/Ge ratio of the gel was varied from 2 to 16, and crystallization kinetics studied using XPD results (Figure S5). The lower the Si/Ge ratio of the gel, the faster CIT-13 crystallized (and the higher the germanium content of the crystals). The CIT-13 crystals typically showed Si/Ge ratios higher than those of the parent gels as shown in Figure S6 (also true for the IM-12 sample, Figure S3). For instance, when the gel Si/Ge ratios were 2, 3, and 4, the Si/Ge ratios of the product, determined using EDS, were 3.84 ± 0.59, 4.72 ± 0.55, and 5.73 ± 0.89, respectively. The amount of water in the gel also affected the crystallization process of CIT-13. We showed previously that a gel with low water content (H_2O/(Si + Ge) = 5) crystallized into CIT-13.[27] Here, three examples of higher water levels (H_2O/(Si + Ge) = 7.5, 10 and 15) were tested, and all resulted in faster crystallization and higher crystallinity. As shown by the data listed in Table 1 and Figure S7, CIT-13 crystallizes with high purity in this range of water content, and the ratios H_2O/(Si + Ge) = 7.5 and 10 appear to be optimal in terms of purity and crystallization rate. The effect of the concentration of the OSDA in the gel on the CIT-13 crystallization was also studied (the amount of HF was also changed molar-equivalently considering the neutralization process, Figure S8). OSDA/(Si + Ge) = 0.5 and 0.625 gave relatively pure CIT-13, but some impurities are discernible as extra peaks in the X-ray diffraction patterns when the OSDA-to-T-atom ratio became higher than 0.75.

The influence of temperature on the crystallization process of CIT-13 was also investigated. As illustrated by the data provided in Figure 3, pure CIT-13 can be synthesized at all temperatures studied: 140, 150, 160, and 175 °C. The crystallization was faster at higher temperatures. At 175 °C, pure CIT-13 was synthesized within 1 week without seeding, whereas at least 4 weeks were required at 140 and 150 °C (Figure S9). Furthermore, an increased crystallization temperature resulted in larger crystals (Figure S10).

3.2. OSDAs for the Crystallization of CIT-13. Previously, we also showed that the position of the methyl group on the benzene ring of benzylimidazolium-derived monoquaternary OSDAs plays an important role in determining which germanosilicate framework is formed.[27] The use of ortho-substituted benzylimidazolium-derivatives resulted in **IWS**-type materials and impure CIT-13, and meta- and para-mono-methyl-substituted benzylimidazolium-derivatives yielded pure CIT-13, and **LTA**-type materials, respectively. Here, the crystallization processes of CIT-13 using three OSDAs that

DOI: 10.1021/acs.chemmater.6b02468
Chem. Mater. 2016, 28, 6250−6259

Table 1. Summary of Synthesis Conditions Tested in This Study, Where All Ratios Are Molar Ratios

OSDA	Si/Ge (gel)	H_2O/T (gel)	(SDA)OH/T and HF/T (gel)	seeding	temperature (°C)	time (days)	major phase
1	4	15	0.5	O	160	28	CIT-13[b]
1	4	15	0.5	X	160	35	CIT-13[b]
1	2	10	0.5	X	160	14	CIT-13[b]
1	3	10	0.5	X	160	14	CIT-13[a]
1	4	10	0.5	O	160	7	CIT-13[a]
1	4	10	0.5	X	160	21	CIT-13[a]
1	8	10	0.5	X	160	21	CIT-13[c]
1	16	10	0.5	X	160	35	CIT-13[c]
1	4	7.5	0.5	O	160	14	CIT-13[b]
1	4	7.5	0.5	X	160	14	CIT-13[a]
1	4	5	0.5	O	160	21	CIT-13[b]
1	4	10	0.5	X	140	28	CIT-13[a]
1	4	10	0.5	X	150	28	CIT-13[a]
1	4	10	0.5	X	175	7	CIT-13[a]
1	4	10	0.625	O	160	14	CIT-13[b]
1	4	10	0.625	X	160	14	CIT-13[b]
1	4	10	0.75	O	160	14	CIT-13[c]
1	4	10	0.75	X	160	14	CIT-13[c]
2	2	10	0.5	X	160	14	CIT-13[c]/**MFI**
2	4	10	0.5	X	160	14	CIT-13[c]/**MFI**
2	8	10	0.5	X	160	14	**MFI**
2	16	10	0.5	X	160	28	**MFI**
2	50	10	0.5	X	160	28	**MFI**
3	2	10	0.5	X	160	21	CIT-13[c]
3	4	10	0.5	X	160	21	CIT-13[c]
3	8	10	0.5	X	160	21	CIT-13[c]
3	16	10	0.5	X	160	56	CIT-13[c]
3	50	10	0.5	X	160	56	amorphous
4	2	10	0.5	X	160	7	CIT-13[a]
4	4	10	0.5	X	160	7	CIT-13[a]
4	8	10	0.5	X	160	14	CIT-13[b]
4	16	10	0.5	X	160	21	CIT-13[b]
4	50	10	0.5	X	160	49	amorphous

[a]CIT-13 purity index: very pure (~100%). [b]CIT-13 purity index: acceptably pure (>95%). [c]CIT-13 purity index: not pure but major phase; the purity was determined qualitatively based on the XPD patterns.

have one or two methyl groups only at the meta-position (OSDA 2–4, Figure 2) were studied for gel Si/Ge ratios ranging from 2 to 50. The XRD profiles in Figure S11–S13 indicate that all four OSDAs promoted the crystallization of CIT-13. Therefore, it can be concluded that methyl group(s) substituted at the meta-position of the OSDA-benzene ring is an important condition for CIT-13 production. Specifically, OSDA 1 and OSDA 4 yielded much purer CIT-13 than did the other two (Figure 4 and S13). OSDA 2 resulted in a mixture of CIT-13 and **MFI**. In a Ge-rich system, CIT-13 was the major phase, whereas **MFI** was the major phase when the gel Si/Ge was high (Figure S11). OSDA 3 also resulted in CIT-13, but one or more impurity phase(s) were observed at all tested gel Si/Ge ratios (Figure S12).

The as-prepared CIT-13 products from OSDA 1 and OSDA 4 were examined using ^{13}C NMR and TGA (Figure 5). The resonances from the solution-phase ^{13}C NMR spectra of OSDA 1 and OSDA 4 match those from the solid-state ^{13}C MAS NMR of as-prepared CIT-13 germanosilicate incorporating each OSDA (Figure 5A), thus showing that the OSDAs were incorporated intact during the synthesis. The TGA curves of as-prepared CIT-13 shown in Figure 5B give approximately 16.5% (OSDA 1) and 15.6% (OSDA 4) weight loss during the temperature ramping from room-temperature to 900 °C. These amounts indicate that a unit cell (64 T atoms) of CIT-13 contains approximately four OSDA molecules (corresponding to 18% weight loss). The refined structure has an OSDA occupancy of only 0.8, giving 3.2 OSDA molecules per unit cell. This corresponds to a weight loss of 15%, which is rather close to the observed amount, and does not include any water that may be occluded in the pores. The less-than-complete occupancy is probably a result of the disorder of the *d*4*r* in the framework structure, and this can vary somewhat from sample to sample. Similar reduced occupancies for the OSDA were also observed in a recent study of SSZ-55 and SSZ-59.[33]

3.3. Use of NH_4F Instead of HF. CIT-13 was also prepared using NH_4F to see if the use of HF could be avoided. CIT-13 samples were prepared using the reference conditions and the molar-equivalent amount of NH_4F salt in place of HF. Ammonia was removed by drying the gel thoroughly using an air flow until the appearance of the gel became very powdery. The crystallization was performed statically in a 160 °C oven. CIT-13 samples prepared in this way were compared with those obtained using HF with XPD, SEM, EDS, TGA, and argon adsorption at 87.45 K. The results are summarized in Figure 6. CIT-13 from the NH_4F-protocol is essentially identical to CIT-13 from the HF-protocol. The XPD profiles (Figure 6A) for both samples show pure CIT-13 with no

DOI: 10.1021/acs.chemmater.6b02468
Chem. Mater. 2016, 28, 6250–6259

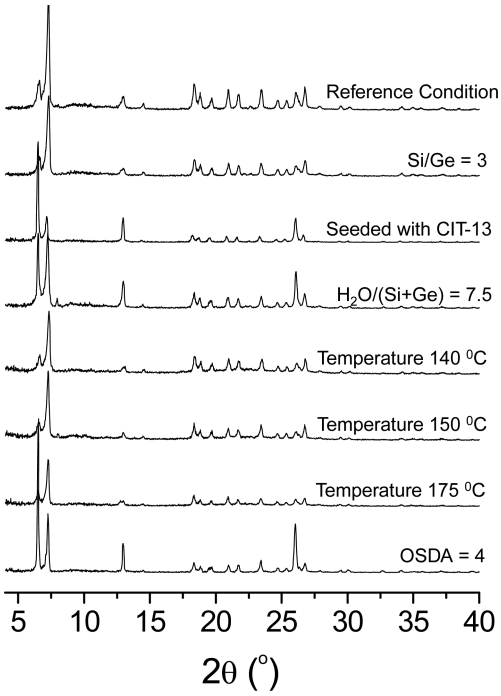

Figure 3. XPD patterns from selected crystallization conditions. The top pattern is from a sample produced under the reference conditions of 0.8 SiO_2:0.2 GeO_2 (Si/Ge = 4):0.5 SDAOH:0.5 HF:10 H_2O at 160 °C without seeding. The effect of varying a specific condition in the synthesis with respect to the reference conditions can be seen in the following patterns.

impurity peaks. The SEM images displayed in Figure 6B and 6C illustrate that the morphologies of the CIT-13 crystals are similar; intergrowth is observed in both samples. The Si/Ge ratios of CIT-13/HF and CIT-13/NH_4F are 5.03 ± 0.48 and 5.19 ± 0.15, respectively. The TGA studies also reveal that the weight loss data are very similar: 16.5% for CIT-13/HF and 16.1% for CIT-13/NH_4F (Figure 6D). The argon adsorption isotherms of the two CIT-13 samples after calcination at 580 °C for 6 h are shown in Figure 6E and are the same. The micropore volumes of CIT-13/NH_4F characterized using the *t*-plot method and the Saito–Foley (SF)-method are 0.191 $cm^3\ g^{-1}$ and 0.215 $cm^3\ g^{-1}$, respectively.

3.4. Structure Analysis of As-Synthesized CIT-13. For structure analysis, a sample of CIT-13 produced using the reference conditions was used. The topology of CIT-13 was obtained from rotation electron diffraction (RED) data[32] using the zeolite-specific program *FOCUS*.[34] Rietveld refinement was initiated in the space group *Cmmm* (a = 13.77 Å, c = 27.32 Å) using the coordinates of the structure for CIT-13 proposed previously[27] and the program *TOPAS*.[35] The background was subtracted manually, and continuously adjusted during the course of the refinement. Framework restraints were put in place, and the framework coordinates were optimized using a geometrical refinement against the restraints. Initial scaling was performed by refining just the scale factor using only the higher angle XPD data, and keeping all other parameters fixed. In a difference electron density map, we expected to find large electron density clouds in the channels corresponding to the position of the OSDA, but instead noticed eight very strong residual peaks reminiscent of a *d4r* and holes on the atoms of the existing *d4r*, indicating that the framework might be disordered. The occupancy of the existing *d4r* was set to 0.5,

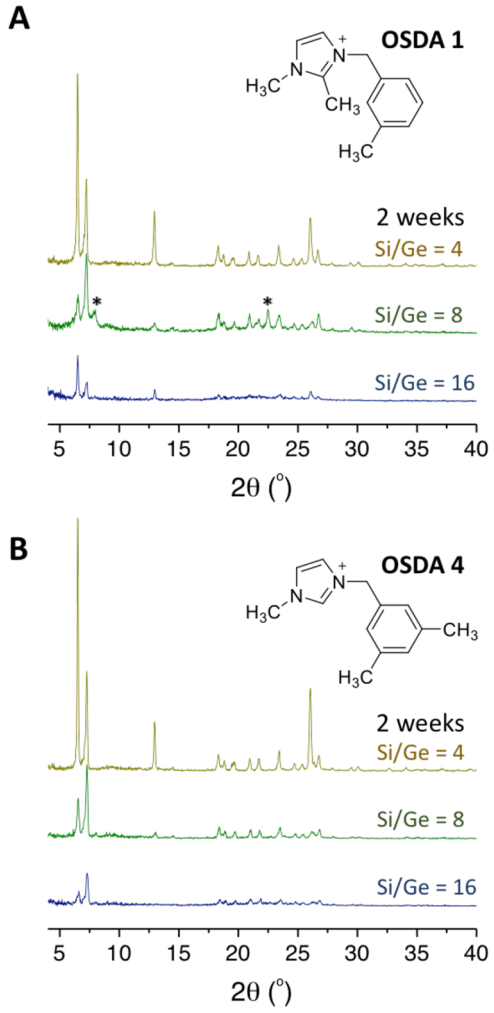

Figure 4. XPD patterns of the samples resulting from different Si/Ge ratios in the gel with (A) OSDA 1 and (B) OSDA 4 for gel compositions $x/(x + 1)$ SiO_2:$1/(x + 1)$ GeO_2:0.5 (OSDA)OH:0.5 HF:10 H_2O where x is the gel Si/Ge ratio. Asterisks (*) denote impurity peaks.

and a second *d4r* was added and constrained to the position of the existing *d4r* with z + 0.5. All Si positions were redefined as mixed Ge/Si positions with a maximum shared occupancy of 1.0 (0.5 in the case of T atoms in the *d4r*). This showed most Ge to be located in the *d4r* units. A subsequent difference map revealed a large smeared out cloud of residual electron density in the center of the channel.

To locate the OSDA in this cloud, a systematic approach that we developed recently was applied.[35] A model of the OSDA was generated and optimized using the energy minimization routine in the program *Jmol*[36] and then added as a rigid body to the *TOPAS* input file. An initial location for the OSDA was found by using the simulated annealing algorithm, by allowing free rotation and translation of the OSDA. The occupancy of the OSDA was allowed to refine as part of this process. The OSDA settled on a position of 8-fold symmetry in the center of the channel intersection with an occupancy of 0.12. This corresponds to a total of almost four OSDA molecules per unit cell, or two per channel intersection. However, with this model, it was not possible to find two OSDA molecules that could be present simultaneously without overlapping.

DOI: 10.1021/acs.chemmater.6b02468
Chem. Mater. 2016, 28, 6250–6259

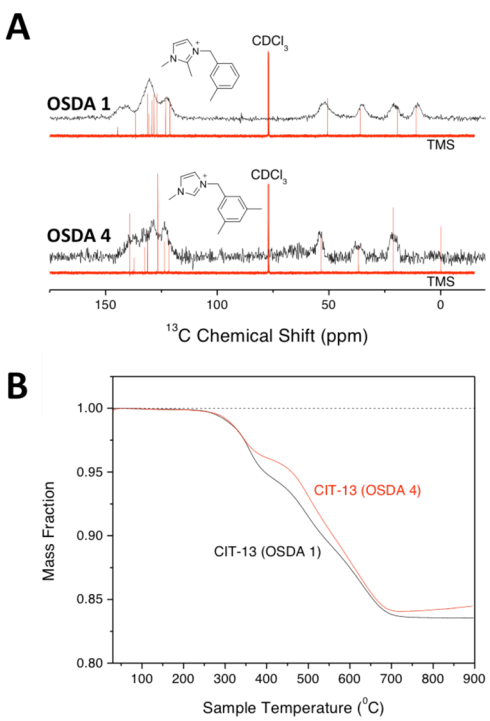

Figure 5. (A) ^{1}H-decoupled ^{13}C solid-state MAS NMR spectra (Black) of CIT-13 samples prepared using OSDA 1 and OSDA 4 with the ^{13}C liquid NMR spectrum (red) of the corresponding OSDA superimposed. (B) TGA profiles of as-prepared CIT-13 synthesized in the presence of OSDA 1 and OSDA 4.

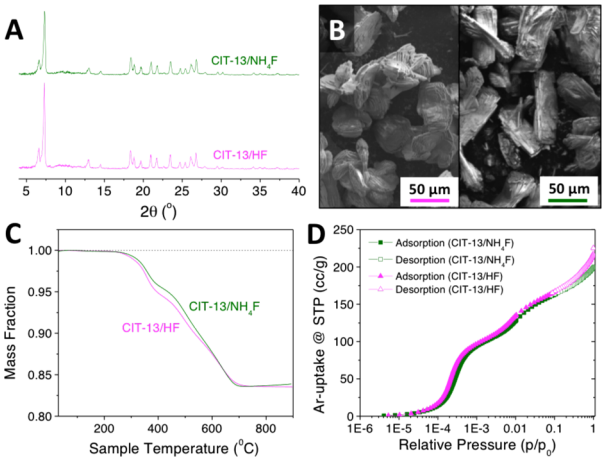

Figure 6. Comparison of the HF and NH_4F protocols for preparing CIT-13. (A) XPD patterns, (B) SEM micrograph images of CIT-13 resulting from the HF (left) and the NH_4F (right) protocols, (C) TGA profiles, and (D) argon adsorption and desorption isotherms at 87.45 K.

It seemed that the most likely case would be two OSDA molecules related by inversion symmetry. Therefore, the symmetry of the structure was lowered to $P\bar{1}$, and the simulated annealing routine was repeated, allowing an additional rotation around the connecting C−N$^+$ bond. However, the simulated annealing routine did not generate any diffraction profiles that matched the observed one. In the next attempt, we set up antibump restraints between the framework oxygen atoms and the C and N atoms of the OSDA, as well as between the C and N atoms of neighboring OSDA molecules, and ran simulated annealing using geometric restraints only. Out of these trials, one model with the imidazole rings facing one another around the inversion point, and the benzyl rings on the other side pointing into the 10-ring windows stood out. The position of the OSDA was transferred to the cell with the original *Cmmm* symmetry, which resulted in a surprisingly good fit to the data.

It is likely that two charged imidazole groups facing one another could give rise to unfavorable interactions, so a similar arrangement with the two benzyl groups facing each other and the imidazole groups pointing into the 10-ring windows was also tested. It was difficult to find a satisfactory position of the OSDA that did not result in very close (<2.5 Å) distances between the framework and the OSDA, or between the OSDAs. A short search of the literature showed that in fact imidazole stacking is not uncommon,[37] so the original position was retained.

Line broadening was treated by applying an anharmonic model.[38] A difference map revealed residual electron density in the middle of the *d4r*, and that was interpreted as F$^-$. The rigid-body model for the OSDA was changed to a geometrically restrained one using the expected bond angles and distances.[39] Antibump restraints were applied to keep the imidazole rings from creeping closer together, and restraints to keep the imidazole and benzyl rings flat were added. Only in the final stages of the refinement was it possible to remove these restraints.

The refinement resulted in a good fit to the data (Figure 7) with agreement values R_I = 0.013 and R_{wp} = 0.077 (R_{exp} = 0.0015). The main differences seem to arise from an anisotropic peak shape that affects some of the reflections. We were unable to find a model to describe this effect completely. The refinement yields a Si/Ge ratio of 5.63. The Ge is located primarily on T7 in the *d4r*, about half of which is Ge. The total occupancy of the OSDAs refined to 0.103, giving a total of 3.26 OSDA molecules per unit cell (out a possible total of 4). Only 2 F$^-$ were found, so we expect the remaining difference in the charge to balance the positively charged OSDA is made up by 1.26 OH$^-$ disordered in the channel system.

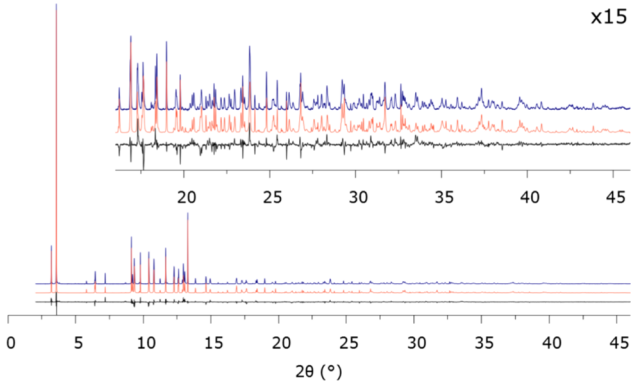

Figure 7. Observed (blue), calculated (red), and difference profiles (black) for the Rietveld refinement of as-prepared CIT-13.

4. DISCUSSION

4.1. Structure. The results of the Rietveld refinement show that the previously proposed framework structure of CIT-13 is partially correct, in that the framework consists of *cfi*-layers interconnected via *d4r* units to form 10- and 14-ring channels

DOI: 10.1021/acs.chemmater.6b02468
Chem. Mater. 2016, 28, 6250−6259

between the layers (Figure 1). In addition, the structure refinement shows that the *d*4*r* units connecting the *cfi*-layers can adopt either of two positions that are related by a translation of 0.5 along the *z* axis. However, their arrangement along the *x* axis is ill-defined, resulting in a disordered framework structure. Two ordered representations (*AAAA* sequence and *ABAB* sequence) are shown in Figure 8. The

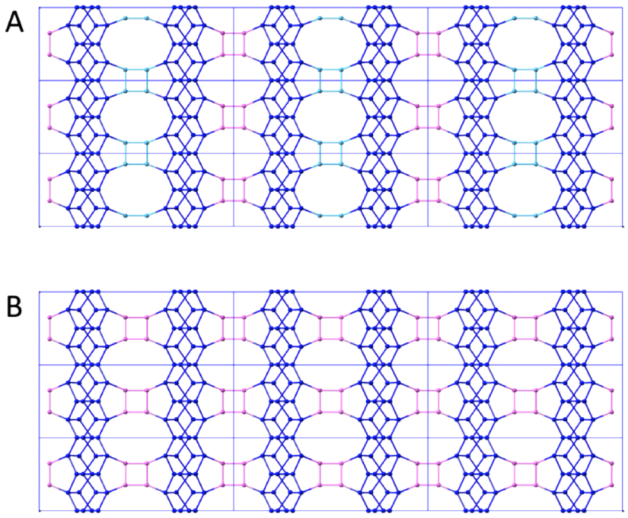

Figure 8. View along *y* showing two stacking possibilities, where the only difference between A and B is the location of the *d*4*r* (pink and light blue). Model A shows an ABAB sequence of *d*4*r*'s while Model B shows an AAAA sequence.

initially proposed structure corresponds to an *AAAA* sequence of *d*4*r* units. Of course, all other sequences of *A* and *B* connections are also possible and this is the cause of the disorder that we observed. However, the XPD data did not show any signs of diffuse scattering or line broadening. We hypothesize that the material consists of medium sized domains (10−20 unit cells) of either *AAAA* or *ABAB* along *x*; however, a definitive answer cannot be given based on XPD data alone.

Another arrangement, in which alternate rows of *d*4*r* units are shifted within the interlayer region, can also be imagined, but this layout is very unfavorable for the OSDA (Figure 9B). The organic cation is either too close to the framework, too close to its neighboring OSDA, or too far from its neighboring OSDA, so that the average occupancy of 0.8 can no longer be reached. Therefore, we believe that disorder within the interlayer region is much less likely than the stacking disorder shown in Figure 8, but it cannot be ruled out completely.

Although the OSDA molecule is also disordered, it seems that two OSDA molecules adopt a supramolecular arrangement at the center of the 14-ring, to carry out their structure-directing effect. The imidazole rings of an OSDA pair are parallel to one another, with a centroid distance of 3.54(1) Å. Each pair can adopt one of four different symmetry-related positions. The methylbenzyl groups on either end of an OSDA pair point into the 10-rings (Figure 9A). The occupancy of the OSDA refines to 0.8, and this allows neighboring OSDA pairs to adopt a different orientation occasionally. The closest distances between the OSDA and the framework are 3.05(1) Å for O10—C13, 3.08(1) Å for O3—C2, 3.09(1) Å for O4—C9, and 3.10(1) Å for O10—C10. All other distances are above 3.1 Å. This has been illustrated with a Hirshfeld surface (Figure 10). The color scheme used on this surface indicates that the

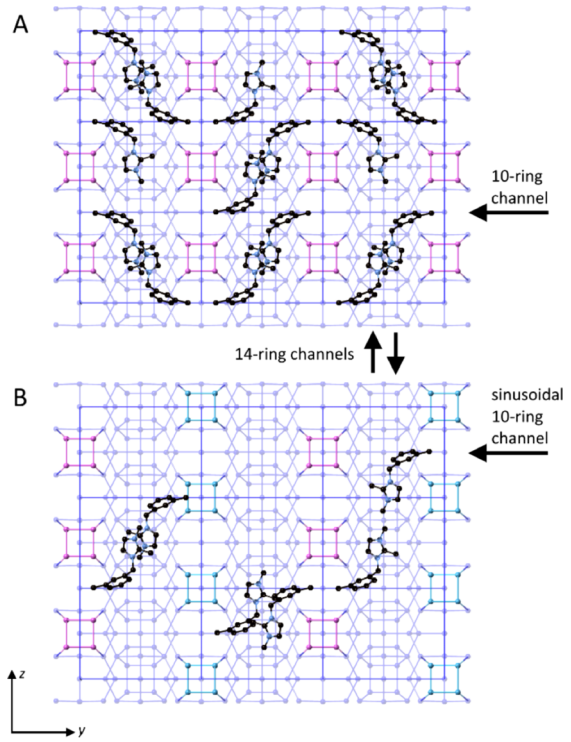

Figure 9. (A) Projection of the structure along x showing a possible arrangement of the OSDA in the refined structure, taking into account that one in five OSDA molecules may be missing. (B) Projection of a theoretically possible framework structure in the *y*−*z*-plane with alternating rows of *d*4*r*'s shifted by one-half along *z*. Three arrangements of pairs of the OSDA molecules based on the refined structure are shown, but none is chemically reasonable.

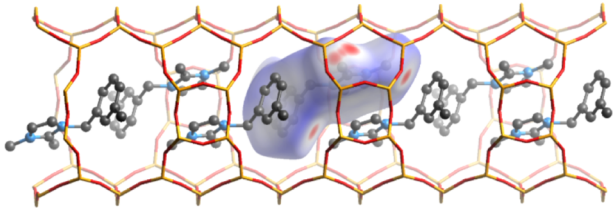

Figure 10. 14-ring channel of CIT-13 (along the *z* axis) viewed down the 10-ring channel (*y* axis), showing the Hirshfeld surface of one OSDA and the arrangement of OSDAs at the intersections of the channels.

contact distances to the framework are either short (red), long (blue), or about equal to the sum of the van der Waals radii (white).

4.2. Comparison between CIT-13 and UTL. Table 2 shows a comparison of the physicochemical data related to the channel and pore systems of IM-12 and CIT-13. The micropore volume found for IM-12 is consistent with the previously reported results.[6,23,40] The micropore volume of CIT-13 is slightly smaller than that of IM-12. This is a reasonable value for CIT-13, because the framework density for CIT-13 (16.41 T atoms nm^{-3}) is higher than that of IM-12 (15.60 T atoms nm^{-3}). The physisorption isotherm of CIT-13 shows two distinct pore filling phenomena in the micropore adsorption region (Figure 11B). We believe that the first pore filling at $p/p_0 \sim 10^{-4}$−10^{-3} arises from the high eccentricity of the 10-ring channels and the second one at $p/p_0 = 10^{-2}$ from the 14-ring channels. The pore size distribution of CIT-13

DOI: 10.1021/acs.chemmater.6b02468
Chem. Mater. 2016, 28, 6250−6259

Table 2. Comparison of Channel and Pore Systems of IM-12 and CIT-13

		IM-12	CIT-13[b]
sample Si-to-Ge ratio[a]		4.5	5.0
space group		*C* 2/*m* (monoclinic)	*Cmmm* (orthorhombic)
framework density (T atoms per nm^3)		15.60	16.41
material density (g cm^{-3})	pure silica	1.56	1.64
	Germanosilicate[a]	1.77	1.84
channel dimension		14-ring	14-ring
		[9.5 × 7.1 Å]	[9.1 × 7.2 Å]
		12-ring	10-ring
		[8.5 × 5.5 Å]	[6.2 × 4.5 Å]
micropore volume (cm^3 g^{-1})	theoretically available[a]	0.376	0.352
	t-plot method	0.177	0.182
	Saito–Foley	0.205	0.222

[a]Calculated based on germanosilicate of the Si/Ge ratio characterized using EDS. [b]Calculated from the crystallographic data from RED (the CIF files are given as Supporting Information).

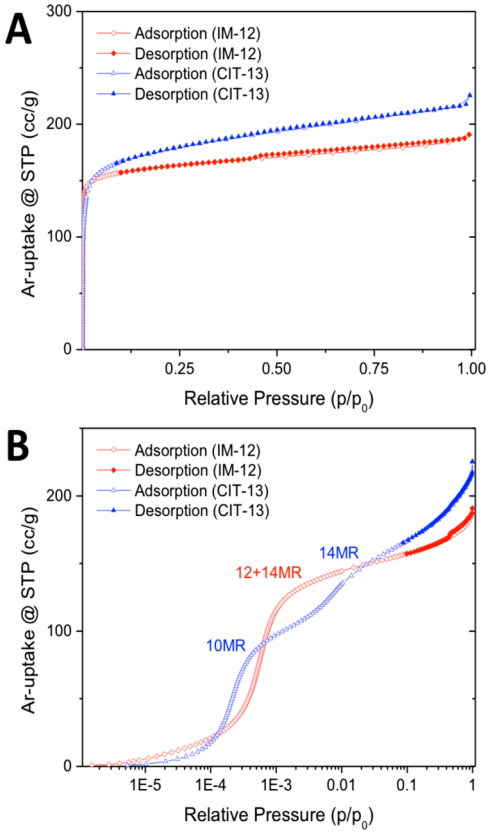

Figure 11. Ar physisorption isotherms at 87 K of calcined CIT-13 and IM-12: (A) linear and (B) log-scale.

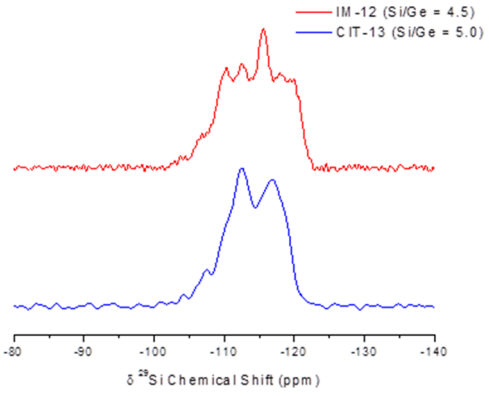

Figure 12. ^{29}Si MAS Solid-state NMR spectra of calcined CIT-13 and IM-12.

according to the cylindrical Saito–Foley model[41] is shown in Figure S14A, and shows two distinct pore-filling steps. This can be attributed to the large size and shape difference between the 10- and 14-ring channels of CIT-13. For IM-12, the dimensions of the 12- and 14-ring channels are not too different from one another, and thus these separated pore-filling steps were not observed.

The ^{29}Si MAS NMR spectra (Figure 12) from the two materials show multiple peaks that significantly overlap with one another in the region from −110 to −120 ppm. The absence of any peaks above −105 ppm indicates that both calcined CIT-13 and IM-12 are composed of Q^4 Si with no significant amounts of silanol groups. IM-12 shows more resonances than CIT-13 in this Q^4 Si-region, indicating that the **UTL** framework has more crystallographically unique T atoms than does ideal CIT-13. Also, there are shoulder-signals in the downfield region from −105 to −110 ppm that can be assigned as either Si atoms residing in the *d4r* units[20,42] or as nSi-(4-n)Ge silicon atoms.[43,44] However, we have not yet been able to make definitive peak-assignments.

5. CONCLUSIONS

The synthesis of the extra-large-pore molecular sieve, CIT-13, with perpendicular intersecting 14- and 10-ring channels was achieved over a wide range of synthetic conditions. Four monoquaternary OSDAs belonging to a family of methyl-benzylimidazolium cations produced CIT-13 as the major phase. The optimized conditions for CIT-13 are as follows: the gel composition at Si/Ge = 3–8, H_2O/T = 5–7.5, $OSDA^+F^-$/T = 0.5 using 1-methyl-3-(3,5-dimethylbenzyl)imidazolium or 1,2-dimethyl-3-(3-methylbenzyl)imidazolium as the OSDA in a static/rotating autoclave in a 140 °C-175 °C oven for 1–3 weeks.

The CIT-13 product was characterized by ^{29}Si MAS NMR and argon adsorption experiments at 87 K and the results were compared with those of IM-12 (**UTL**). Calcined CIT-13 showed a ^{29}Si NMR spectrum largely similar to that of calcined IM-12, with no silanol groups detected. However, the calcined CIT-13 sample produced a two-step argon adsorption isotherm in the low pressure range, indicating that the adsorption behavior inside the 10-ring channel is very different to that of

DOI: 10.1021/acs.chemmater.6b02468
Chem. Mater. 2016, 28, 6250–6259

the 14-ring channel of IM-12. This type of isotherm was not observed for IM-12. The micropore volume from the *t*-plot method was 0.18−0.19 $cm^3\ g^{-1}$.

A synthesis protocol using NH_4F instead of HF was developed and the material from that protocol characterized. The CIT-13 solids obtained via the two protocols were essentially the same, thus effectively providing a way of avoiding the use of concentrated hydrogen fluoride.

We analyzed the structure of CIT-13 using high-resolution synchrotron XPD data. Using Rietveld refinement, we were able to sort out the disorder present in the framework structure, to determine the positions of Ge in the framework, and to locate the extra-framework species in the channels and cavities. The OSDA adopts a pairwise supramolecular arrangement at the center of the 14-ring. As in other studies of germanosilicates, we found that Ge is located primarily in the *d4r* unit, making it a suitable starting material for transformations via the ADOR process.

■ ASSOCIATED CONTENT

Supporting Information

The Supporting Information is available free of charge on the ACS Publications website at DOI: 10.1021/acs.chemmater.6b02468.

Schematic diagrams of the frameworks structures, supplementary XPD patterns and SEM images, adsorption isotherms, additional crystallographic information on CIT-13. (PDF)

Crystal Data of As-Synthesized CIT-13 from Rietveld Refinement (CIF)

Idealized Model of As-Synthesized CIT-13 (for visualization) (CIF)

Crystal Data of Framework-Only CIT-13 from Rotational Electron Diffraction (CIF)

■ AUTHOR INFORMATION

Corresponding Author

*E-mail: mdavis@cheme.caltech.edu.

Author Contributions

The manuscript was written through contributions of all authors. All authors have given approval to the final manuscript.

Notes

The authors declare no competing financial interest.

■ ACKNOWLEDGMENTS

We thank Chevron Energy and Technology Company for support of this research. We thank Dr. Joel Schmidt for useful comments throughout the research study. We thank Antonio Cervellino for his assistance with the powder diffraction measurement on the Materials Science Beamline at the SLS in Villigen, Switzerland. This work was supported also by the Swiss National Science Foundation.

■ REFERENCES

(1) Davis, M. E. Ordered porous materials for emerging applications. *Nature* **2002**, *417*, 813−821.

(2) Schmidt, J. E.; Xie, D.; Rea, T.; Davis, M. E. CIT-7, a crystalline, molecular sieve with pores bounded by 8 and 10-membered rings. *Chem. Sci.* **2015**, *6*, 1728−1734.

(3) Li, J.; Corma, A.; Yu, J. Synthesis of new zeolite structures. *Chem. Soc. Rev.* **2015**, *44*, 7112−7127.

(4) Jiang, J.; Yu, J.; Corma, A. Extra-Large-Pore Zeolites: Bridging the Gap between Micro and Mesoporous Structures. *Angew. Chem., Int. Ed.* **2010**, *49*, 3120−3145.

(5) Maesen, T. The zeolite scene — an overview. In *Stud. Surf. Sci. Catal.*; Jiří Čejka, H. v. B. A. C., Ferdi, S., Eds.; Elsevier, 2007; Vol. *168*, Ch. 1, pp 1−12.

(6) Shvets, O. V.; Zukal, A.; Kasian, N.; Žilková, N.; Čejka, J. The Role of Crystallization Parameters for the Synthesis of Germanosilicate with UTL Topology. *Chem. - Eur. J.* **2008**, *14*, 10134−10140.

(7) O'Keeffe, M.; Yaghi, O. M. Germanate Zeolites: Contrasting the Behavior of Germanate and Silicate Structures Built from Cubic T8O20 Units (T = Ge or Si). *Chem. - Eur. J.* **1999**, *5*, 2796−2801.

(8) Blasco, T.; Corma, A.; Díaz-Cabañas, M. J.; Rey, F.; Vidal-Moya, J. A.; Zicovich-Wilson, C. M. Preferential Location of Ge in the Double Four-Membered Ring Units of ITQ-7 Zeolite. *J. Phys. Chem. B* **2002**, *106*, 2634−2642.

(9) Corma, A.; Diaz-Cabanas, M. J.; Rey, F.; Nicolopoulus, S.; Boulahya, K. ITQ-15: The first ultralarge pore zeolite with a bidirectional pore system formed by intersecting 14- and 12-ring channels, and its catalytic implications. *Chem. Commun.* **2004**, 1356−1357.

(10) Corma, A.; Diaz-Cabanas, M. J.; Jorda, J. L.; Martinez, C.; Moliner, M. High-throughput synthesis and catalytic properties of a molecular sieve with 18- and 10-member rings. *Nature* **2006**, *443*, 842−845.

(11) Sun, J.; Bonneau, C.; Cantin, A.; Corma, A.; Diaz-Cabanas, M. J.; Moliner, M.; Zhang, D.; Li, M.; Zou, X. The ITQ-37 mesoporous chiral zeolite. *Nature* **2009**, *458*, 1154−1157.

(12) Corma, A.; Díaz-Cabañas, M. J.; Jiang, J.; Afeworki, M.; Dorset, D. L.; Soled, S. L.; Strohmaier, K. G. Extra-large pore zeolite (ITQ-40) with the lowest framework density containing double four- and double three-rings. *Proc. Natl. Acad. Sci. U. S. A.* **2010**, *107*, 13997−14002.

(13) Jiang, J.; Jorda, J. L.; Yu, J.; Baumes, L. A.; Mugnaioli, E.; Diaz-Cabanas, M. J.; Kolb, U.; Corma, A. Synthesis and Structure Determination of the Hierarchical Meso-Microporous Zeolite ITQ-43. *Science* **2011**, *333*, 1131−1134.

(14) Jiang, J.; Jorda, J. L.; Diaz-Cabanas, M. J.; Yu, J.; Corma, A. The Synthesis of an Extra-Large-Pore Zeolite with Double Three-Ring Building Units and a Low Framework Density. *Angew. Chem., Int. Ed.* **2010**, *49*, 4986−4988.

(15) Jiang, J.; Yun, Y.; Zou, X.; Jorda, J. L.; Corma, A. ITQ-54: a multi-dimensional extra-large pore zeolite with 20 [times] 14 [times] 12-ring channels. *Chem. Sci.* **2015**, *6*, 480−485.

(16) Paillaud, J.-L.; Harbuzaru, B.; Patarin, J.; Bats, N. Extra-Large-Pore Zeolites with Two-Dimensional Channels Formed by 14 and 12 Rings. *Science* **2004**, *35*, 990−992.

(17) Guth, J. L.; Kessler, H.; Wey, R. New Route to Pentasil-Type Zeolites Using a Non Alkaline Medium in the Presence of Fluoride Ions. In *Studies in Surface Science and Catalysis*; Y. Murakami, A. I., Ward, J. W., Eds.; Elsevier B.V.: Amsterdam, 1986; Vol. *28*, pp 121−128.

(18) Corma, A.; Puche, M.; Rey, F.; Sankar, G.; Teat, S. J. A Zeolite Structure (ITQ-13) with Three Sets of Medium-Pore Crossing Channels Formed by9- and 10-Rings. *Angew. Chem., Int. Ed.* **2003**, *42*, 1156−1159.

(19) Gao, F.; Jaber, M.; Bozhilov, K.; Vicente, A.; Fernandez, C.; Valtchev, V. Framework Stabilization of Ge-Rich Zeolites via Postsynthesis Alumination. *J. Am. Chem. Soc.* **2009**, *131*, 16580−16586.

(20) Xu, H.; Jiang, J.-g.; Yang, B.; Zhang, L.; He, M.; Wu, P. Post-Synthesis Treatment gives Highly Stable Siliceous Zeolites through the Isomorphous Substitution of Silicon for Germanium in Germanosilicates. *Angew. Chem., Int. Ed.* **2014**, *53*, 1355−1359.

(21) El-Roz, M.; Lakiss, L.; Vicente, A.; Bozhilov, K. N.; Thibault-Starzyk, F.; Valtchev, V. Ultra-fast framework stabilization of Ge-rich zeolites by low-temperature plasma treatment. *Chem. Sci.* **2014**, *5*, 68−80.

(22) Verheyen, E.; Joos, L.; Van Havenbergh, K.; Breynaert, E.; Kasian, N.; Gobechiya, E.; Houthoofd, K.; Martineau, C.; Hinterstein,

DOI: 10.1021/acs.chemmater.6b02468
Chem. Mater. 2016, 28, 6250−6259

M.; Taulelle, F.; Van Speybroeck, V.; Waroquier, M.; Bals, S.; Van Tendeloo, G.; Kirschhock, C. E. A.; Martens, J. A. Design of zeolite by inverse sigma transformation. *Nat. Mater.* **2012**, *11*, 1059−1064.
(23) Roth, W. J.; Nachtigall, P.; Morris, R. E.; Wheatley, P. S.; Seymour, V. R.; Ashbrook, S. E.; Chlubná, P.; Grajciar, L.; Položij, M.; Zukal, A.; Shvets, O.; Čejka, J. A family of zeolites with controlled pore size prepared using a top-down method. *Nat. Chem.* **2013**, *5*, 628−633.
(24) Shamzhy, M.; Opanasenko, M.; Tian, Y.; Konysheva, K.; Shvets, O.; Morris, R. E.; Čejka, J. Germanosilicate Precursors of ADORable Zeolites Obtained by Disassembly of ITH, ITR, and IWR Zeolites. *Chem. Mater.* **2014**, *26*, 5789−5798.
(25) Baerlocher, C.; McCusker, L. B.; Olson, D. H. *Atlas of Zeolite Framework Types* 6th ed.; Elsevier B.V.: Amsterdam, 2007; pp 371.
(26) Mazur, M.; Wheatley, P. S.; Navarro, M.; Roth, W. J.; Položij, M.; Mayoral, A.; Eliášová, P.; Nachtigall, P.; Čejka, J.; Morris, R. E. Synthesis of 'unfeasible' zeolites. *Nat. Chem.* **2015**, *8*, 58−62.
(27) Boal, B. W.; Deem, M. W.; Xie, D.; Kang, J. H.; Davis, M. E.; Zones, S. I. Synthesis of Germanosilicate Molecular Sieves from Mono- and Di-Quaternary Ammonium OSDAs Constructed from Benzyl Imidazolium Derivatives: Stabilization of Large Micropore Volumes Including New Molecular Sieve CIT-13. *Chem. Mater.* **2016**, *28*, 2158−2164.
(28) Wagner, P.; Yoshikawa, M.; Tsuji, K.; Davis, M. E.; Wagner, P.; Lovallo, M.; Taspatsis, M. CIT-5: a high-silica zeolite with 14-ring pores. *Chem. Commun.* **1997**, 2179−2180.
(29) Lobo, R. F.; Tsapatsis, M.; Freyhardt, C. C.; Khodabandeh, S.; Wagner, P.; Chen, C.-Y.; Balkus, K. J.; Zones, S. I.; Davis, M. E. Characterization of the Extra-Large-Pore Zeolite UTD-1. *J. Am. Chem. Soc.* **1997**, *119*, 8474−8484.
(30) Shvets, O. V.; Kasian, N.; Zukal, A.; Pinkas, J.; Čejka, J. The Role of Template Structure and Synergism between Inorganic and Organic Structure Directing Agents in the Synthesis of UTL Zeolite. *Chem. Mater.* **2010**, *22*, 3482−3495.
(31) Bergamaschi, A.; Cervellino, A.; Dinapoli, R.; Gozzo, F.; Henrich, B.; Johnson, I.; Kraft, P.; Mozzanica, A.; Schmitt, B.; Shi, X. The MYTHEN detector for X-ray powder diffraction experiments at the Swiss Light Source. *J. Synchrotron Radiat.* **2010**, *17*, 653−668.
(32) Wan, W.; Sun, J.; Su, J.; Hovmoller, S.; Zou, X. Three-dimensional rotation electron diffraction: software RED for automated data collection and data processing. *J. Appl. Crystallogr.* **2013**, *46*, 1863−1873.
(33) Smeets, S.; McCusker, L. B.; Baerlocher, C.; Elomari, S.; Xie, D.; Zones, S. Locating Organic Guests in Inorganic Host Materials from X-ray Powder Diffraction Data. *J. Am. Chem. Soc.* **2016**, *138*, 7099−7106.
(34) Smeets, S.; McCusker, L. B.; Baerlocher, C.; Mugnaioli, E.; Kolb, U. Using FOCUS to solve zeolite structures from three-dimensional electron diffraction data. *J. Appl. Crystallogr.* **2013**, *46*, 1017−1023.
(35) Coelho, A. A. *TOPAS-ACADEMIC*, v 5.0; Coelho Software: Brisbane, Australia, 2012.
(36) Hanson, R. Jmol - a paradigm shift in crystallographic visualization. *J. Appl. Crystallogr.* **2010**, *43*, 1250−1260.
(37) De, S.; Drew, M. G. B.; Aliaga-Alcalde, N.; Datta, D. Imidazole−imidazole stacking in some inorganic complexes. *Inorg. Chim. Acta* **2009**, *362*, 2879−2883.
(38) Stephens, P. Phenomenological model of anisotropic peak broadening in powder diffraction. *J. Appl. Crystallogr.* **1999**, *32*, 281−289.
(39) Cowley, J. M.; Peng, L. M.; Ren, G.; Dudarevc, S. L.; Whelanc, M. J. Parametrizations of Electron Atomic Scattering Factors. In *International Tables for Crystallography*; E. Prince; John Wiley & Sons, Inc.: Hoboken, NJ, 2006; p 262.
(40) Chlubná, P.; Roth, W. J.; Greer, H. F.; Zhou, W.; Shvets, O.; Zukal, A.; Čejka, J.; Morris, R. E. 3D to 2D Routes to Ultrathin and Expanded Zeolitic Materials. *Chem. Mater.* **2013**, *25*, 542−547.
(41) Saito, A.; Foley, H. C. Curvature and parametric sensitivity in models for adsorption in micropores. *AIChE J.* **1991**, *37*, 429−436.
(42) Rojas, A.; Camblor, M. A. A Pure Silica Chiral Polymorph with Helical Pores. *Angew. Chem., Int. Ed.* **2012**, *51*, 3854−3856.
(43) Shamzhy, M. V.; Shvets, O. V.; Opanasenko, M. V.; Yaremov, P. S.; Sarkisyan, L. G.; Chlubna, P.; Zukal, A.; Marthala, V. R.; Hartmann, M.; Cejka, J. Synthesis of isomorphously substituted extra-large pore UTL zeolites. *J. Mater. Chem.* **2012**, *22*, 15793−15803.
(44) Kasian, N.; Vanbutsele, G.; Houthoofd, K.; Koranyi, T. I.; Martens, J. A.; Kirschhock, C. E. A. Catalytic activity and extra-large pores of germanosilicate UTL zeolite demonstrated with decane test reaction. *Catal. Sci. Technol.* **2011**, *1*, 246−254.

DOI: 10.1021/acs.chemmater.6b02468
Chem. Mater. 2016, 28, 6250−6259